Biophysical Journal
Article

Biophysical Society

Suppression of L_α/L_β Phase Coexistence in the Lipids of Pulmonary Surfactant

Jonathan R. Fritz,[1] Ryan W. Loney,[2] Stephen B. Hall,[2,*] and Stephanie Tristram-Nagle[1,*]
[1]Biological Physics Group, Department of Physics, Carnegie Mellon University, Pittsburgh, Pennsylvania and [2]Pulmonary and Critical Care Medicine, Oregon Health & Science University, Portland, Oregon

ABSTRACT To determine how different constituents of pulmonary surfactant affect its phase behavior, we measured wide-angle x-ray scattering (WAXS) from oriented bilayers. Samples contained the nonpolar and phospholipids (N&PL) obtained from calf lung surfactant extract (CLSE), which also contains the hydrophobic surfactant proteins SP-B and SP-C. Mixtures with different ratios of N&PL and CLSE provided the same set of lipids with different amounts of the proteins. At 37°C, N&PL by itself forms coexisting L_α and L_β phases. In the L_β structure, the acyl chains of the phospholipids occupy an ordered array that has melted by 40°C. This behavior suggests that the L_β composition is dominated by dipalmitoyl phosphatidylcholine (DPPC), which is the most prevalent component of CLSE. The L_β chains, however, lack the tilt of the $L_{\beta'}$ phase formed by pure DPPC. At 40°C, WAXS also detects an additional diffracted intensity, the location of which suggests a correlation among the phospholipid headgroups. The mixed samples of N&PL with CLSE show that increasing amounts of the proteins disrupt both the L_β phase and the headgroup correlation. With physiological levels of the proteins in CLSE, both types of order are absent. These results with bilayers at physiological temperatures indicate that the hydrophobic surfactant proteins disrupt the ordered structures that have long been considered essential for the ability of pulmonary surfactant to sustain low surface tensions. They agree with prior fluorescence micrographic results from monomolecular films of CLSE, suggesting that at physiological temperatures, any ordered phase is likely to be absent or occupy a minimal interfacial area.

SIGNIFICANCE The ability of pulmonary surfactant to reduce alveolar surface tension is essential for preserving the integrity of the lungs during normal breathing. The experiments here provided detailed structural information for hydrated bilayers of extracted calf surfactant at precisely controlled physiological temperatures. Wide-angle x-ray scattering determined chain order in the complete set of surfactant lipids with and without the hydrophobic surfactant proteins. The results are analogous to prior micrographic findings from monolayers of the same material. Our results question whether an ordered phase, long thought to be essential for surfactant function, is present in monomolecular films containing the full complement of constituents under physiological conditions.

INTRODUCTION

Phase behavior was proposed long ago to play a crucial role in the function of pulmonary surfactant. This mixture of phospholipids with small amounts of cholesterol and protein forms a thin film on the surface of the liquid layer that lines the alveolar air sacs of the lungs (1). When compressed by the shrinking alveolar surface area during exhalation, the film reduces the surface tension of the air/liquid interface to exceptionally low levels, <5 mN/m (2–6). Monomolecular films that are fluid fail to reach these low surface tensions during compression at physiological rates. At the equilibrium spreading tension (γ_e), at which a monolayer coexists with its bulk phase (7), compressed fluid films collapse from the surface to reestablish equilibrium interfacial densities. The low alveolar surface tensions indicate that the alveolar films must resist flow from the interface. They must have the rheological characteristics of a solid.

Dipalmitoyl phosphatidylcholine (DPPC), which is the most prevalent constituent of pulmonary surfactant from most animals (8), forms solid films. At physiological temperatures and the γ_e, monolayers of DPPC occur as the tilted-condensed (TC) phase (9). The acyl chains occupy a centered, rectangular lattice in a tilted configuration, equivalent to the leaflets in the $L_{\beta'}$ phase of bilayers. DPPC monolayers readily replicate the performance of the alveolar film,

Submitted October 2, 2020, and accepted for publication December 7, 2020.
*Correspondence: sbh@ohsu.edu or stn@cmu.edu
Editor: Georg Pabst.
https://doi.org/10.1016/j.bpj.2020.12.008

undergoing slow compression to low surface tensions (10). This classical model of pulmonary surfactant predicts that the alveolar film is condensed, with a composition dominated by DPPC (11,12).

Early speculation also suggested that phase behavior might determine the kinetics of forming the alveolar film (11,12). Vesicles of $L_{\beta'}$ phospholipids, such as DPPC at physiological temperatures, adsorb poorly (13–15). DPPC represents ~35% of the surfactant mixture (16). Early models proposed that the other constituents disrupt ordered structures and produce fluid bilayers that adsorb quickly (11,12). Subsequent evidence has shown that disordering of lipids does not necessarily produce rapid adsorption. L_{α} vesicles composed only of phospholipids adsorb slowly and incompletely (17–19). Whether the constituents other than DPPC, however, disrupt the ordered structures that are central to the classical model remains uncertain.

Testing the structural predictions of the classical model has been difficult. The structural phases present in any system depend on the intensive variables. The important variables for interfacial films are surface tension, or surface pressure, and temperature. Experiments that provide structural information on films of pulmonary surfactant at physiological temperatures near γ_e have been difficult. Measurements with Wilhelmy balances may achieve γ_e but usually at ambient laboratory temperatures. The few microscopic studies conducted near physiological conditions have suggested that an ordered phase is present but that it occupies a minimal fraction of the interface (20). Grazing incidence x-ray diffraction (GIXD) provides more definitive information by detecting diffraction from acyl chains in a crystalline lattice. GIXD detects an ordered phase in surfactant monolayers, but experiments have only obtained data at ambient temperatures, far below physiological levels (21,22).

The studies reported here used wide-angle x-ray scattering (WAXS) to obtain structural information from oriented bilayers of extracted calf surfactant. X-ray diffuse scattering (XDS) from oriented multibilayers provides a high signal-to-noise ratio that allows analysis of well-defined coexisting phases. Structures obtained with multilamellar and unilamellar systems are equivalent, eliminating concerns that interactions with adjacent bilayers might distort structures (23). The chamber containing the samples (23) fully hydrates bilayers and easily achieves physiological temperatures. WAXS, like GIXD, can detect diffraction from acyl chains in a crystalline lattice. The structure of a bilayer may well correspond to a monolayer with a surface pressure at or above the equilibrium spreading pressure (π_e) (24). We tested whether the ordered structures predicted by the classical model are present at physiological temperatures in the surfactant bilayers and the role of different constituents in determining those structures.

MATERIALS AND METHODS

Materials

HPLC grade chloroform, trifluoroethanol, and methanol were obtained from Thermo Fischer Scientific (Pittsburgh, PA). The constituents of calf lung surfactant extract (CLSE), provided by ONY Biotech (Amherst, NY), were obtained by extracting (25) phospholipid aggregates lavaged from freshly excised calf lungs (26). Subfractions of the constituents in CLSE were obtained by established methods (27) based on gel permeation chromatography (28,29). These procedures yielded the complete set of nonpolar and phospholipids (N&PL) without the surfactant proteins SP-B and SP-C. Cholesterol constitutes essentially all of the nonpolar lipids. Concentrations of the proteins and phospholipids were determined by colorimetric assays (30,31), using bovine serum albumin as the standard protein. The content of the proteins (32), their physical constants (Table 1), and the composition of the lipids (16,27,34,35) in CLSE are all known. SP-B and SP-C represent ~1.5% (w/w) (~500:1 lipid/protein molar ratio) of the complete mixture (32).

Mixtures of N&PL and CLSE in different molar ratios provided the same set of surfactant lipids with different amounts of the hydrophobic proteins. The two preparations were mixed in solutions of organic solvents as follows: 4 mg mixture in 200 μL chloroform:trifluoroethanol (TFE) (1:1, v:v). The ratio of N&PL and CLSE was expressed as the mole fraction of phospholipid contributed by CLSE: X_{CLSE} = CLSE/(CLSE + N&PL).

Methods

Our experiments measured x-ray scattering from oriented films of the different mixtures. The samples were plated onto silicon wafers (15 × 1.5 × 30 mm^3) using the rock-and-roll method (36), in which continuous rocking of the silicon wafer during solvent evaporation produces stacks of ~1800 well-aligned bilayers. Once immobile, further solvent was evaporated for at least 2 h. The sample was trimmed to a central 5-mm strip parallel to the long edge of the wafer (36). A thick-walled, well-insulated chamber containing MilliQ water in its base maintained 100% humidity that hydrated the 10-μm-thick films (23). Samples were equilibrated for 30 min after reaching the experimental temperature. Hydration of the samples by the vapor preserves sample orientation, which is lost in lipids dispersed in excess water.

Data collection and analysis

Most measurements used the G1 line at the Cornell High Energy Synchrotron Source (CHESS; Cornell University, Ithaca, NY) to obtain XDS from oriented, hydrated samples during two separate visits using wavelengths of 1.1775 and 1.0976 Å. The distances from sample to detector (S-distance) for WAXS were 173 and 159 mm, respectively, and 365.1 and 417.0 mm for low-angle x-ray scattering (LAXS). Additional experiments collected WAXS using a Rigaku RUH3R rotating anode x-ray source with a wavelength of 1.5418 Å and S-distance of 126.7 mm.

Our experiments determined both WAXS and LAXS on the same films. Lowering the beamstop allowed measurements of LAXS, which determined lamellar D-spacing, or the repeat distance of the stacked bilayers. For LAXS, the flat silicon wafers supporting the films were rotated at

TABLE 1 Physical Constants for Bovine SP-B and SP-C

Protein	SP-B (dimer)	SP-C
Molecular mass (Da)	17,397	4,042
Number of amino acids	158	34
Net charge (e′)	+12	+2
Weight ratio	1	1
Molar ratio	0.21	1

(32,33).

20°/s from −1.6 to 7° during the 1-s scans to obtain all scattered x-rays equally. The first and second strong lamellar orders indicated the D-spacing according to the Bragg equation.

WAXS provided d-spacing, or the distance between acyl chains. Dezingered scans were first collected for 30 s, with the beam incident at an angle of 0.5°, followed by a second scan collected at −0.5°. Scattering from the sample did not occur during this second scan. Subtraction of these two images, therefore, removed all background scattering from air, water vapor, and mylar. To obtain a profile of intensities, the background-subtracted images were first imported into MATLAB (Version 2009; The MathWorks, Natick, MA). The variation of intensity from $q_r = 0$ to 1.8 Å^{-1} was obtained using a horizontal swath with a vertical q_z height of Δq_z = 0.07 Å^{-1}, centered at $q_z \approx 0.2$ Å^{-1}. These intensities were then plotted using MATLAB's plottera function and exported as an ASCII file. The profiles of scattered intensity were imported into OriginPro (OriginLab, Northampton, MA), in which they were truncated at low and high q_r and subsequently superimposed onto the WAXS image (Figs. 2, 3, and 8). These traces were also used to calculate the areas under the relevant peaks.

The WAXS from various samples included a narrow peak that corresponded to the L_β phase and a broad signal from a more disordered structure. For the L_β peak, we obtained the full width at half maximum (FWHM) and d-spacing using MATLAB's sector plot function by taking a discrete step of a radial swath, 5–10° from the equator, from the background-subtracted WAXS images. After importing the profiles of intensities into OriginPro, a baseline was subtracted. A multipeak function then fit the profile, with two Gaussian distributions to describe the contributions of the two most prevalent peaks. Because the scattering images at $X_{CLSE} = 0.0$ and 0.1 were indistinguishable, the visual representations in Figs. 2, 3, and 8 omitted the images at $X_{CLSE} = 0.1$.

To determine whether the broad peak in the WAXS represented coexisting phases, we fit the radial variation of the intensities with models that assumed one or two structures. The analysis, described previously (37,38), uses liquid-crystal theory to model the order of the lipid chains with a Maier-Saupe distribution of tilt angles. The order of the lipid chains determines the variation of radial intensity with the angle, φ, from the image's equator (39). Visually superior fitting with two distributions rather than one supports the presence of coexisting phases.

RESULTS

LAXS

Our experiments determined the structural role of lipids other than DPPC and of the hydrophobic surfactant proteins SP-B and SP-C. Samples of N&PL, with the full complement of surfactant lipids, determined how lipids other than DPPC affected the well-known structure formed by that compound. CLSE, with the hydrophobic proteins as well as the lipids, then determined the effect of those proteins.

LAXS at full hydration produced diffuse lobes of scattered intensity (Fig. 1 *A*). Two or three orders of diffraction were evident through the semitransparent molybdenum beamstop (Fig. 1 *B*). The peaks corresponded to a single lamellar phase. Calculation of lamellar D-spacing with the Bragg equation showed that values were essentially invariant to changes in X_{CLSE} (Fig. 1 *C*). Up to physiological levels, the proteins had no effect on the repeat distance for the stacked bilayers.

LAXS can also provide information on the hydration of bilayers. Oriented films that achieve the same D-spacing as multilamellar vesicles in excess water demonstrate that the lipids are fully hydrated. That comparison was unavailable here because of the behavior of the surfactant lipids. During progressive hydration, multilamellar vesicles of zwitterionic phospholipids swell to a finite, maximal D-spacing, which then remains constant with further hydration. Samples containing anionic phospholipids, such as N&PL and CLSE (16,27,35), can swell without limit because of electrostatic repulsion, which leads to the absence of diffraction (39,40). The lack of well-defined values of D-spacing for our samples when dispersed in excess water complicated efforts to show that our films achieved full hydration.

An alternative approach provided reassurance. We calculated the number of water molecules associated with our samples using the equation $A \times D = 2\,(V_L + n_W V_W)$, where A = area/lipid, D = lamellar D-spacing, V_L = volume/lipid, n_W is the number of water molecules/lipid, and V_W = volume of a water molecule at 37°C (24). Based on recently published values of A and V_L for these samples (41), we calculated that the largest D-spacing of 77 Å in Fig. 1 yielded $n_W \approx 70$; the smallest D-spacing of 63 Å indicated $n_W \approx 43$. Both values of n_W are well above 35, which was the largest n_W for the zwitterionic egg phosphatidylcholine (24). Lobes of XDS only appear from oriented samples of L_α within ~5 Å of full hydration (42). The presence of those lobes with our samples and the calculated values of n_W both support ample hydration in our experiments.

WAXS

In contrast to LAXS, which displayed a single D-spacing, WAXS demonstrated phase coexistence (Fig. 2, *top left*

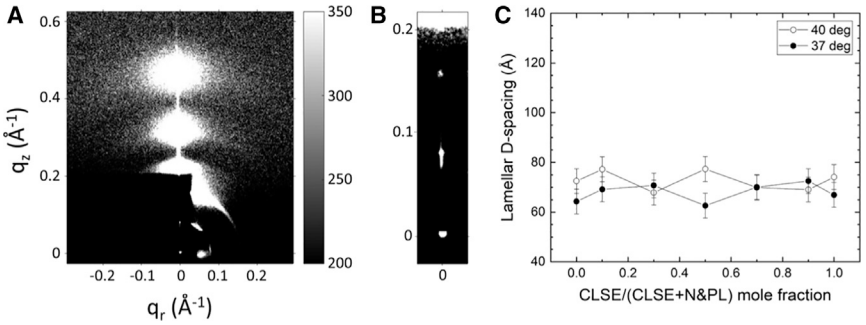

FIGURE 1 XDS from N&PL/CLSE multibilayers. (*A*) LAXS from fully hydrated samples is shown. The narrow vertical strip to the right of the image gives the conversion of measured intensity (arbitrary units) to grayscale in the image. (*B*) Two lamellar orders of LAXS visible with adjusted greyscale through the semi-transparent molybdenum beamstop are shown. Note the different ranges of q_z for images (*A*) and (*B*). (*C*) Lamellar D-spacing of N&PL/CLSE bilayers at 37 and 40°C at different X_{CLSE}. Symbols here and elsewhere give mean ± SD.

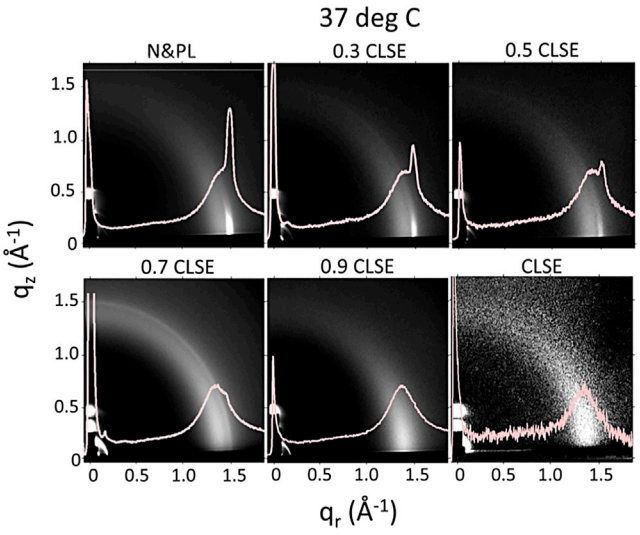

FIGURE 2 WAXS at 37°C from mixtures of N&PL/CLSE with increasing X_{CLSE}. The pattern from LAXS is evident at the lower left, partially covered by the dark, rectangular beamstop. The superimposed light traces give the horizontal profiles of the intensity as a function of q_r. Greyscale was optimized to display the L_β peak. To see this figure in color, go online.

panel), with two distinct distributions of intensity at well-separated d-spacings. The scattered intensity included both a sharp, intense peak at $q_r \approx 1.5$ Å^{-1} located on the equator at $q_z = 0$ Å^{-1} and a much broader peak at $q_r \approx 1.4$ Å^{-1}. The single, sharp peak on the equator indicated hexagonal packing without tilt of the acyl chains. These findings define the L_β phase and distinguish it from the $L_{\beta'}$ structure formed by DPPC, in which the chains are tilted. The $L_{\beta'}$ phase produces a sharp, off-equatorial (1,1) reflection in addition to the (2,0) equatorial reflection in Fig. 2 (43). At physiological temperatures, the lipids in pulmonary surfactant other than DPPC removed the tilt of the acyl chains from the $L_{\beta'}$ structure but not the crystalline array. At 40°C (Fig. 3, *top left panel*), close to the temperature at which bilayers of pure DPPC melt to L_α, the L_β phase was absent. The higher temperature eliminated the ordered structure in N&PL.

The broader peak at $q_r \approx 1.4$ Å^{-1} for N&PL at 37°C is characteristic of the L_α phase. The presence of cholesterol and a phospholipid with a high melting transition, however, raised the possibility that the liquid-ordered (L_o) phase might also be present. To test for coexisting L_α and L_o phases, we analyzed the radial variation of scattering. Liquid-crystal theory describes how the distribution of tilt by the acyl chains should affect the scattered intensity and its radial variation (37,38). A single distribution provided an excellent fit to the data for N&PL at both 37 and 40°C (Fig. 4). Inclusion of a second distribution failed to improve the fit. A single disordered phase explained the data.

The profile from N&PL at 40°C (Fig. 3) contained an additional faint, broad peak at $q_r \approx 0.82$ Å^{-1}. The value of q_r indicated that the signal resulted from a structure with a repeat distance of ~7.7 Å. The lateral size of a phospholipid headgroup, obtained from the square root of the area per lipid (24), approximated that distance. For N&PL, correlation of the headgroups provided the most reasonable explanation of the weak H-peak at low q_r.

Our experiments also tested how the hydrophobic surfactant proteins altered the phase behavior of the lipids. CLSE added to N&PL varied X_{CLSE} and increased the amount of the hydrophobic proteins present with the same set of lipids. At 37°C, increasing X_{CLSE} progressively decreased the intensity of the sharp L_β signal (Figs. 2 and 5). With larger amounts of the SPs, the radial extension of the sharp peak decreased (e.g., $X_{CLSE} = 0.7$), consistent with greater misorientation. At $X_{CLSE} = 0.9$, the L_β signal was absent (Fig. 2). The profile of intensity only showed the broad peak from the disordered phase (Fig. 2). For pure CLSE at $X_{CLSE} = 1.0$ and 37°C, increased noise (Fig. 2) resulted in a weaker signal, but the L_β peak was clearly missing. At physiological temperatures, physiological levels of the proteins eliminated formation of the L_β phase by the surfactant lipids.

As expected, the L_β peak, which was absent for N&PL at 40°C, was similarly missing at that temperature for the samples with protein. Increasing concentrations of the proteins diminished the prominence of the H-peak (Fig. 3). The integrated area under the H-peak (Fig. 6) showed that the signal persisted to $X_{CLSE} = 0.9$. For the complete physiological mixture, however, the H-peak was absent (Figs. 3 and 6). These results indicated that, at 40°C, the proteins disrupted any long-range ordering of the lipid headgroups.

X_{CLSE} had minimal effect on the peak position, q_r, for either L_α or L_β (Fig. 7). When both phases were present at 37°C, the d-spacing for the L_α phase was significantly

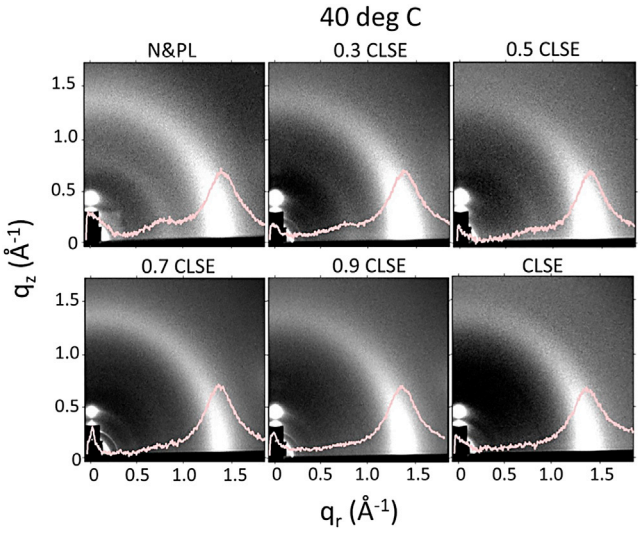

FIGURE 3 WAXS at 40°C of N&PL mixtures with increasing X_{CLSE}. The pattern from LAXS is evident at the lower left, partially covered by the dark, rectangular beamstop. The superimposed light traces give the horizontal profiles of the intensity with q_r. Greyscale is optimized to display the H-peak at $q_r \approx 0.8$ Å^{-1}. To see this figure in color, go online.

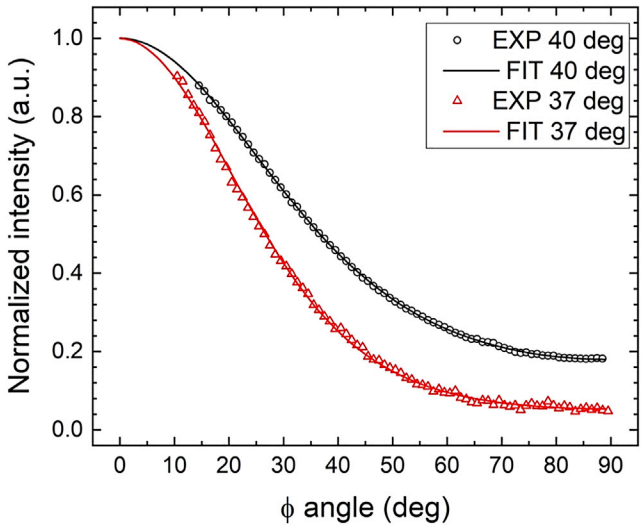

FIGURE 4 Radial plot of the intensity from the broad WAXS peak in N&PL at 37 and 40°C. The symbols give experimental (EXP) intensities; solid lines (FIT) are the best fit of a liquid-crystal model to the data with a single decay. Intensities are normalized for each case to the value at $\varphi = 0°$ for ease of viewing. To see this figure in color, go online.

greater than for L_β. The value for L_β was constant, independent of X_{CLSE} (Fig. 7). Over the range of X_{CLSE} from 0.0 to 1.0, d-spacing of the L_α phase increased by 2%, which approached the accuracy of the measurements (± 0.5 Å). At 40°C, at which only the L_α phase was present, the proteins had no effect on d-spacing (Fig. 7). The small amounts of protein present in pulmonary surfactant achieved the disruption of the L_β phase and headgroup correlation without a major shift in the separation of the chains.

The effect of the proteins indicated that CLSE sits close to, but outside of, the L_α/L_β coexistence region. That

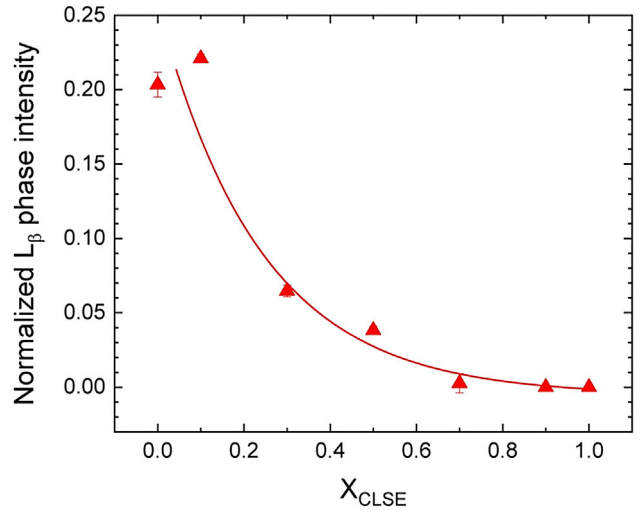

FIGURE 5 L_β intensity normalized relative to the disordered phase at 37°C as a function of increasing X_{CLSE}. Some SDs are smaller than the symbols. The solid line uses an exponential fit to guide the eye. To see this figure in color, go online.

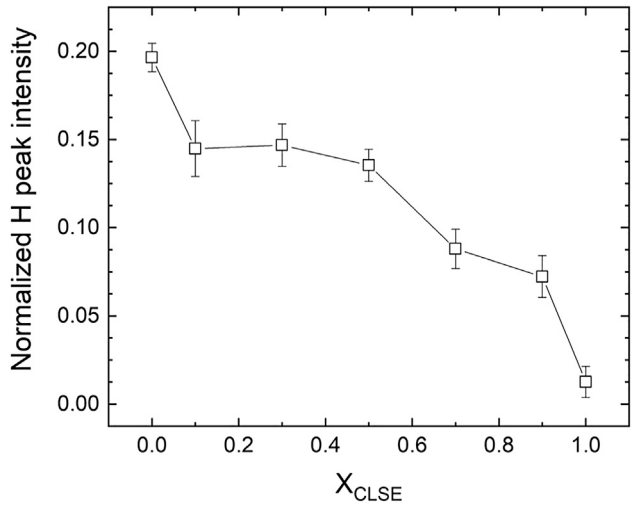

FIGURE 6 Intensity of the H-peak normalized to the disordered phase at 40°C as a function of increasing X_{CLSE}.

observation suggested that coexistence, although absent at 37°C, might occur at slightly lower temperatures. We tested that possibility by measuring WAXS from oriented films of CLSE during cooling. Because CHESS was inaccessible during the severe acute respiratory syndrome coronavirus 2 (SARS-CoV-2) pandemic, we conducted those experiments with a rotating anode source rather than the synchrotron. The noise in these images (Fig. 8) was consequently greater than for our measurements at the synchrotron.

The results emphasized the importance of temperature. L_α/L_β coexistence was evident for CLSE at 33°C and more pronounced at 29 and 26°C (Fig. 8). The quantitated intensity from the L_β peak demonstrated a nearly linear increase with decreasing temperatures (Fig. 9). At 26°C, the L_β intensity reached ~70% of the value for the L_α phase, well above the ratio of 20% for N&PL at 37°C. These findings indicated that, under physiological conditions, the amount of the proteins is just sufficient to suppress L_α/L_β coexistence. Even a small decrease in temperature allowed formation of the L_β phase.

The width of the diffraction peaks from a crystalline structure can provide the size of regions that produce coherent scattering. According to the Scherrer equation (44), the diameter of crystalline domains, τ, is given by:

$$\tau = \frac{\kappa \lambda}{\beta \cos(\theta)}, \tag{1}$$

where κ is the unitless shape factor ~0.9, λ is the x-ray wavelength in Angstroms, β is the FWHM in radians, and θ is the Bragg angle of the peak. To correct for instrumental resolution, we subtracted the FWHM for the beam from the raw value for the WAXS peak. X_{CLSE} had essentially no effect on β for the L_β structure at 37°C, which remained effectively constant at 0.3° (Fig. 10). Prior microscopic studies of CLSE monolayers (20) suggest that the ordered phase forms

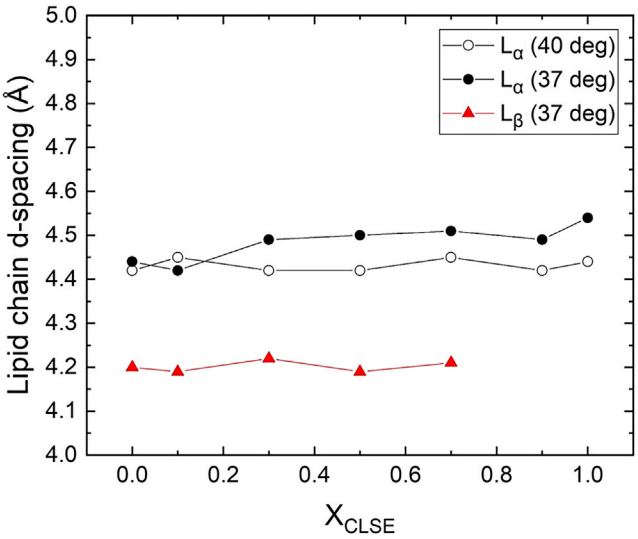

FIGURE 7 Lipid chain d-spacings for L_α and L_β phases at 37 and 40°C as a function of increasing X_{CLSE}. The SD of these measurements is ±0.05 Å. To see this figure in color, go online.

roughly circular domains surrounded by a continuous disordered film. Calculations, here, using a circular shape yielded L_β regions with an area of ~340 nm^2 (Fig. 11). Based on calculations of the area per acyl chain ((43); Eq. 3), the area per molecule for the L_β phase should be ~41 $Å^2$. The

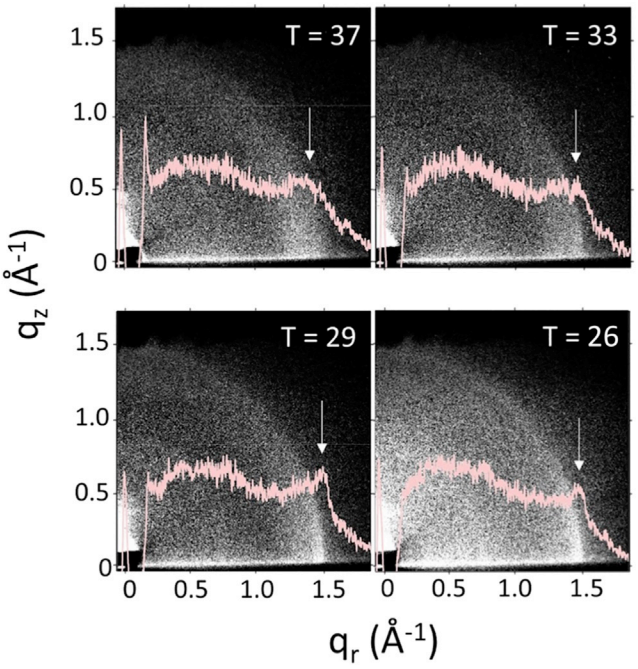

FIGURE 8 WAXS of CLSE as a function of temperature (°C). The pattern from LAXS is evident at the lower left, partially covered by the rectangular beamstop. The superimposed light traces give the horizontal profiles of the intensity as a function of q_r . White arrows indicate the location of the L_β peak. Greyscale is optimized to display the L_β peak. To see this figure in color, go online.

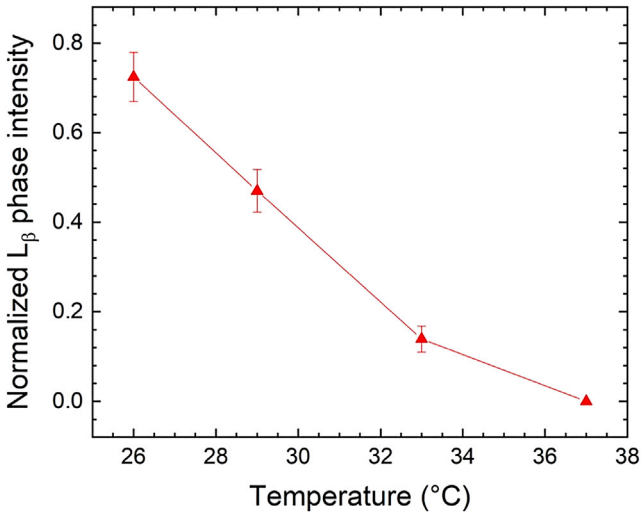

FIGURE 9 WAXS intensity from the L_β phase for CLSE normalized to the L_α phase as a function of temperature. To see this figure in color, go online.

L_β domains would contain ~800 phospholipids, irrespective of the amount of protein present.

DISCUSSION

Structural effects

Lipids other than DPPC

LAXS from our samples with the surfactant lipids detected a single D-spacing, superficially suggesting a single lamellar phase. Two structures, however, can also produce a single D-spacing because of frustration (37). Competition for the available water can yield a common spacing as a compromise. In the out-of-plane, vertical direction measured by

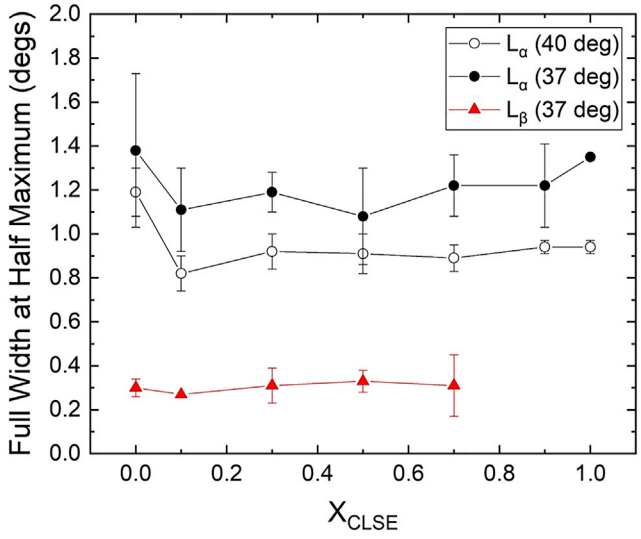

FIGURE 10 Full width at half maximum (FWHM) of L_α and L_β phase peaks at 37 and 40°C as a function of increasing X_{CLSE}. To see this figure in color, go online.

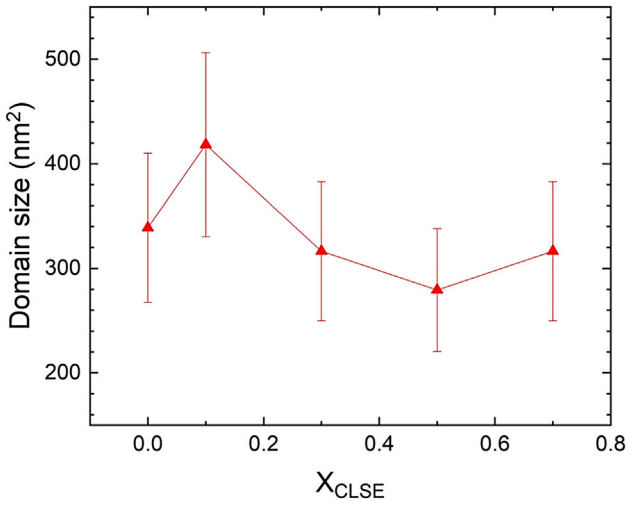

FIGURE 11 Dimensions of the L_β domains calculated using the Scherrer equation, as a function of increasing X_{CLSE}. The error bars were calculated using errors in d-spacing and FWHM. To see this figure in color, go online.

LAXS, neither structure has a coherence length sufficient to yield a distinct D-spacing. WAXS, instead, detects in-plane spacings where the coherence lengths are great enough to distinguish the two d-spacings found here.

WAXS shows that, at 37°C, bilayers of the surfactant lipids contain regions of the L_β phase. At that temperature, the only constituent that can form a comparable structure by itself is DPPC. That compound forms a $L_{\beta'}$ phase that transitions to an L_α structure at ~41°C (45,46). The ordered chains of N&PL melt between 37 and 40°C. These results support an ordered phase at the lower temperature that contains predominantly DPPC.

The L_β structure formed by the surfactant lipids differs from the $L_{\beta'}$ phase of pure DPPC. The tilt of the chains in $L_{\beta'}$ is absent from L_β. These results resemble findings by GIXD from monolayers of CLSE. At 23°C and surface pressures below 40 mN/m, the films contain ordered structures with the centered rectangular unit cell of the TC phase, comparable with the leaflets of the $L_{\beta'}$ bilayers (21,22). Compression to 44 mN/m, however, converts the structure to the hexagonal lattice of the untitled condensed phase, comparable to the structures found here (22). The greater compression removes the tilt of the acyl chains.

The structural difference between the L_β phase and the $L_{\beta'}$ of pure DPPC indicates that the ordered regions contain other compounds. The two possibilities are cholesterol and the phospholipids other than DPPC. Our current experiments provide no insight into which constituents are more likely to produce the structural difference. Prior studies have shown that, in simple ternary mixtures, both unsaturated phospholipids and cholesterol can remove the tilt from the chains of DPPC (47). Studies with monolayers of the surfactant lipids support inclusion of cholesterol with DPPC in the ordered phase (48,49), but provide no information concerning the other phospholipids.

The L_β phase in the surfactant lipids coexists with disordered regions. The composition of these lipids, which contain high- and low-melting phospholipids along with cholesterol, suggest that they might form coexisting L_α and L_o phases. The following three criteria argue for a single disordered phase and against phase coexistence (38): LAXS detects peaks corresponding to a single D-spacing; a single disordered phase coexisting with the L_β regions accounts for the profile of WAXS; a single distribution of tilt for the acyl chains explains the radial dependence of the WAXS. No findings suggest coexistence in the disordered regions.

Two arguments suggest that the single disordered phase is L_α rather than L_o. First, the shape of the imaged WAXS differs from the roughly circular, equatorial pattern of intensities normally seen with the L_o phase (37). Second, ternary mixtures of DPPC/dioleoyl phosphatidylcholine (DOPC)/cholesterol at 35°C formed L_o structures only at cholesterol contents >10% (mol:mol) (50), above the level of 8% (mol:mol) present here (27). The available evidence suggests that bilayers of the surfactant lipids form coexisting L_α and L_β phases at 37°C and the L_α phase alone at 40°C.

The bilayers also contain a structure that produces a faint, broad H-peak at 40°C but not at 37°C. We speculate that the difference between the two temperatures may reflect the phase behavior. The diffracting structure must have a coherence length long enough to produce coherent interference. At 40°C, the L_α phase is present alone. The L_α/L_β phase coexistence at 37°C generates domains of discrete dimensions. The domains may interrupt the structure that generates the H-peak. The shortened coherence length may eliminate this weak signal.

Prior studies have observed a signal with a similar q_r. The structures that produced the signal in those studies should be different from the source of our H-peak. The similar signal occurs with bilayers of DPPC (51) and monolayers of glycosylphosphatidylinositols (52) when each is present as the subgel phase. The headgroup-headgroup interaction in the highly ordered subgel is associated with crystalline acyl chains. Our H-peak occurs only at 40°C, where the L_α phase is present alone. The correlation of headgroups in our samples occurs without the associated ordering of the acyl chains.

Hydrophobic surfactant proteins

The physiological mixture of the hydrophobic surfactant proteins produces a dose-dependent disordering of the surfactant lipids. The proteins disrupt the L_β phase at 37°C, as well as the structure that produces the H-peak at 40°C. At physiological levels, despite the small amounts of proteins present (~500:1 lipid:protein molar ratio in CLSE), both structures are gone. The proteins achieve their disordering effect, at least for the L_β phase, without affecting the size of the ordered domains. Based on the width of the WAXS peaks, the domains remain approximately the

same size with different amounts of the proteins. The standard deviations (SD) of our results are significant (Fig. 11). Within that uncertainty, the proteins eliminate the L_β domains by decreasing their number rather than reducing their size.

Functional correlates

Adsorption

The original view of pulmonary surfactant considered its composition as consisting of DPPC with other constituents (11,12). DPPC would form the solid interfacial monolayer that would resist collapse during compression to low surface tensions. The other constituents would disrupt solid structures in freshly secreted vesicles and allow rapid adsorption to the interface. Our results show that lipids other than DPPC partially achieve this disordering function. N&PL includes a disordered phase that should be fluid, and that is absent at 37°C in bilayers of pure DPPC. The other lipids also alter the ordered structure formed by DPPC. That change, however, is relatively minor, confined to the tilt of the chains. The ordered packing of the chains persists. The other lipids are unable to disrupt the ordered structure proposed to limit adsorption.

At physiological levels, the proteins prevent formation of the L_β phase by the surfactant lipids. According to the original view (11,12), the elimination of the ordered phase by the proteins would explain their dramatic effect on adsorption. This explanation of how the proteins achieve their essential function is unlikely. The critical change would be conversion of the lipids from L_α/L_β coexistence to a homogeneous L_α bilayer. That mechanism would predict that other L_α vesicles would adsorb rapidly. Relative to the phospholipid with the hydrophobic proteins, DOPC by itself, in the L_α phase at temperatures well above its main transition, adsorbs slowly and incompletely (17–19). Elimination of an interfacial boundary between coexisting L_α and L_β phases also has little effect on adsorption (34,53). The proteins could facilitate adsorption by making the lipids more fluid. To the best of our knowledge, that possibility remains untested. The rheological effects of the proteins are unknown. Disruption of the L_β phase by itself, however, seems inadequate to explain how the proteins promote adsorption.

Stability of the interfacial film

Our results with the surfactant bilayers seem more likely to provide insights into the behavior of the alveolar film than to explain how surfactant vesicles adsorb. Many investigators have considered that phase behavior determines the resistance to collapse of the compressed alveolar film. The classical model and its variants predict that a monomolecular alveolar film must include an ordered phase that resists collapse. The functionally important structure would be present at the equilibrium spreading pressure (π_e) of 46 mN/m (13–15), at which collapse can begin, and at a temperature in mammals of ~37°C. Providing detailed structural information at those conditions has been difficult. The experiments here easily achieve physiological temperatures. Leaflets of a bilayer may have a structure equivalent to monolayers at a surface pressure different from π_e, but the temperature is appropriate.

The existing literature, however, suggests that the "bilayer equivalence pressure," at which the monolayer most closely mimics the structure of the bilayer, may approach or exceed π_e (10,54–56). Isobaric monolayers held at constant surface pressure melt from the TC phase to disordered structures over a narrow range of temperatures, analogous to the melting of phases in bilayers. The melting temperature depends on surface pressure. These curves show that DPPC monolayers melt at ~41°C, the temperature of the main transition for $L_{\beta'}$ bilayers of that compound, when surface pressure is 45 mN/m (10). The most widely accepted equivalence pressure is 30–35 mN/m (57), significantly below the π_e of 46 mN/m. The simple correspondence of the melting behaviors supports a higher value. The structures at 37°C in monolayers at π_e and bilayers may be quite similar.

The temperature dependence of the ordered structure in our bilayers supports that possibility. In monolayers of CLSE, coexistence begins at surface pressures that increase with temperature (20). At higher temperatures, the gap between the onset of coexistence and π_e narrows. At π_e, the ordered phase, which grows during compression across that gap, is progressively smaller. The behavior of the ordered phase in monolayers at π_e and bilayers is similar. At progressively higher temperatures, the extent of the ordered phase decreases in both structures. At 37°C, the ordered structure is absent or minimally present. The similar temperature dependence supports the structural similarity of leaflets in the bilayer with monolayers at π_e.

Our results agree with a challenge to a major corollary of the classical model. That model suggests that the alveolar film has a structure equivalent to the leaflets of a bilayer in the gel phase (11,12). DPPC is the only constituent of pulmonary surfactant that by itself forms an ordered phase at physiological temperatures (8,16). DPPC constitutes ~35% of the complete mixture (16). The presence of the other components has suggested that for the film to become functional its composition must change. The squeeze-out hypothesis proposes that compression above π_e selectively excludes compounds other than DPPC (11). Current evidence indicates that phospholipids collapse regionally rather than as individual compounds (58,59). For a film with L_α/L_β coexistence, compression excludes the disordered phase, generating a mostly ordered film (60). Prior microscopic studies (20), supported by our current results, indicate that an ordered phase is absent when collapse should begin. These findings eliminate the basis for forming the functional

film by selective exclusion. The condensed film of the classical model might form by some other process, but not by selective collapse.

Our results also argue against a possible solution to this problem. Under conditions at which fluorescence microscopy detects limited condensed phase in surfactant monolayers (20), atomic force microscopy (AFM) shows numerous nanoscopic domains (61). Together with ordered microscopic regions, these structures occupy almost half of the interface. This difference raises the possibility that fluorescence microscopy may fail to detect an ordered phase because of inadequate spatial resolution. The agreement between WAXS and fluorescence microscopy argues against that possibility. The measurements with WAXS should at least approach the resolution of AFM. WAXS, like fluorescence microscopy, detects few or no ordered structures at physiological conditions. The disparity between the studies with the two microscopic methods seems more likely to reflect compositional or methodological differences rather than the ability to detect existing structures.

The preponderance of data here and published elsewhere (20,62) raise significant questions concerning the classical model and its variants. Under physiological conditions, the full complement of interfacially active constituents favors structures that are homogeneously disordered or that lie within but perilously close to the boundary of an ordered/disordered coexistence region. The structure proposed to explain the stability of the alveolar film is either absent or minimally present. The results suggest that the model fails to acknowledge some functionally important factor. The current literature suggests three possibilities:

1) Curvature: Recent studies show that the configuration of discontinuous ordered domains in films related to pulmonary surfactant changes on tightly curved surfaces (63). The domains become highly asymmetric. In a system with progressively growing discontinuous domains, such as compressed films of CLSE (20), the change in shape could shift the percolation threshold at which the discontinuous domains form a continuous network. The shift could explain how domains that occupy a minor fraction of the interface provide the basis for resisting collapse of a curved alveolar film. The model suggests, however, that films of pulmonary surfactant should become stable at low surface tension only on the highly curved interfaces where the striped phase forms. Experimental evidence contradicts that prediction (64–67).
2) Multilamellar films: Several groups have shown that surfactant films on modestly curved surfaces collapse slowly when the subphase contains surfactant vesicles (64–67). Electron micrographs show that at least portions of the alveolar film are multilamellar rather than monomolecular (68,69). The greater thickness of the multilamellar film might slow rates of collapse (70). Formation of an interfacial multilayer by vesicles in the subphase might then explain their stabilizing effect. Direct measurements on the thickness of initial adsorbed films have produced conflicting results concerning the presence of additional layers (22,71).
3) Compositional change: An alternative explanation for the effect of material in the subphase is that the vesicles might change the composition of the interfacial film (66). Partitioning of DPPC between adjacent vesicles and the surface might enrich the interfacial content of that compound. The ordered structures predicted by the classical model that resist collapse might then form with the different composition.

CONCLUSION

WAXS shows that the complete set of surfactant lipids forms bilayers with two ordered structures. At 37°C, the L_β phase, in which the acyl chains of the phospholipids occupy an ordered lattice, differs from the $L_{\beta'}$ phase formed by pure DPPC only in the absence of tilt by the chains. The higher temperature of 40°C melts the L_β phase, but a structure with the cross section of the headgroup produces a faint H-peak. The hydrophobic surfactant proteins produce a dose-dependent disruption of both ordered structures. At physiological temperatures and levels of the proteins, the samples form only the L_α phase. This observation has significant implications for the mechanisms by which alveolar films achieve their characteristic low surface tensions.

AUTHOR CONTRIBUTIONS

J.R.F. performed the experiments with the rotating anode, analyzed data, and wrote the manuscript. R.W.L. prepared the samples and collected WAXS data at the CHESS synchrotron. S.B.H. designed the experiments and wrote the manuscript. S.T.-N. supervised the collection of x-ray data and their analysis and wrote the manuscript.

ACKNOWLEDGMENTS

The authors thank Yasmene Elhady, Diamond Moody, Akari Kumagai, Megan Roche, John Nagle, and Horia Petrache for help in collecting data at CHESS, and John Nagle for helpful discussions.

These studies were supported by the National Institutes of Health (HL060914, HL130130, and HL136734). The Cornell High Energy Synchrotron Source was supported by the National Science Foundation under award number DMR-1332208.

REFERENCES

1. Goerke, J., and J. A. Clements. 1985. Alveolar surface tension and lung surfactant. *In* Handbook of Physiology - The Respiratory System, Part 1 P. T. Macklem and J. Mead, eds. Volume III. American Physiological Society, pp. 247–261.
2. Horie, T., and J. Hildebrandt. 1971. Dynamic compliance, limit cycles, and static equilibria of excised cat lung. *J. Appl. Physiol.* 31:423–430.

3. Schürch, S., J. Goerke, and J. A. Clements. 1976. Direct determination of surface tension in the lung. *Proc. Natl. Acad. Sci. USA.* 73:4698–4702.
4. Valberg, P. A., and J. D. Brain. 1977. Lung surface tension and air space dimensions from multiple pressure-volume curves. *J. Appl. Physiol.* 43:730–738.
5. Wilson, T. A. 1981. Relations among recoil pressure, surface area, and surface tension in the lung. *J. Appl. Physiol.* 50:921–930.
6. Smith, J. C., and D. Stamenovic. 1986. Surface forces in lungs. I. Alveolar surface tension-lung volume relationships. *J. Appl. Physiol.* 60:1341–1350.
7. Gaines, G. L., Jr. 1966. Insoluble Monolayers at Liquid-Gas Interfaces. Interscience Publishers, New York, p. 147.
8. Postle, A. D., E. L. Heeley, and D. C. Wilton. 2001. A comparison of the molecular species compositions of mammalian lung surfactant phospholipids. *Comp. Biochem. Physiol. A Mol. Integr. Physiol.* 129:65–73.
9. Kaganer, V. M., H. Möhwald, and P. Dutta. 1999. Structure and phase transitions in Langmuir monolayers. *Rev. Mod. Phys.* 71:779–819.
10. Crane, J. M., G. Putz, and S. B. Hall. 1999. Persistence of phase coexistence in disaturated phosphatidylcholine monolayers at high surface pressures. *Biophys. J.* 77:3134–3143.
11. Clements, J. A. 1977. Functions of the alveolar lining. *Am. Rev. Respir. Dis.* 115 (6 part 2):67–71.
12. Bangham, A. D., C. J. Morley, and M. C. Phillips. 1979. The physical properties of an effective lung surfactant. *Biochim. Biophys. Acta.* 573:552–556.
13. Tajima, K., and N. L. Gershfeld. 1978. Equilibrium studies of lecithin-cholesterol interactions. II. Phase relations in surface films: analysis of the "condensing" effect of cholesterol. *Biophys. J.* 22:489–500.
14. Lee, S., D. H. Kim, and D. Needham. 2001. Equilibrium and dynamic interfacial tension measurements at microscopic interfaces using a micropipet technique. 2. Dynamics of phospholipid monolayer formation and equilibrium tensions at water-air interface. *Langmuir.* 17:5544–5550.
15. Mansour, H. M., and G. Zografi. 2007. Relationships between equilibrium spreading pressure and phase equilibria of phospholipid bilayers and monolayers at the air-water interface. *Langmuir.* 23:3809–3819.
16. Kahn, M. C., G. J. Anderson, …, S. B. Hall. 1995. Phosphatidylcholine molecular species of calf lung surfactant. *Am. J. Physiol.* 269:L567–L573.
17. Biswas, S. C., S. B. Rananavare, and S. B. Hall. 2005. Effects of gramicidin-A on the adsorption of phospholipids to the air-water interface. *Biochim. Biophys. Acta.* 1717:41–49.
18. Biswas, S. C., S. B. Rananavare, and S. B. Hall. 2007. Differential effects of lysophosphatidylcholine on the adsorption of phospholipids to an air/water interface. *Biophys. J.* 92:493–501.
19. Loney, R. W., W. R. Anyan, …, S. B. Hall. 2011. The accelerated late adsorption of pulmonary surfactant. *Langmuir.* 27:4857–4866.
20. Discher, B. M., K. M. Maloney, …, S. B. Hall. 1996. Lateral phase separation in interfacial films of pulmonary surfactant. *Biophys. J.* 71:2583–2590.
21. Alonso, C., F. Bringezu, …, J. A. Zasadzinski. 2005. Modifying calf lung surfactant by hexadecanol. *Langmuir.* 21:1028–1035.
22. Andreev, K., M. W. Martynowycz, …, D. Gidalevitz. 2020. Structural changes in films of pulmonary surfactant induced by surfactant vesicles. *Langmuir.* 36:13439–13447.
23. Kučerka, N., Y. Liu, …, J. F. Nagle. 2005. Structure of fully hydrated fluid phase DMPC and DLPC lipid bilayers using X-ray scattering from oriented multilamellar arrays and from unilamellar vesicles. *Biophys. J.* 88:2626–2637.
24. Nagle, J. F., and S. Tristram-Nagle. 2000. Structure of lipid bilayers. *Biochim. Biophys. Acta.* 1469:159–195.
25. Bligh, E. G., and W. J. Dyer. 1959. A rapid method of total lipid extraction and purification. *Can. J. Biochem. Physiol.* 37:911–917.
26. Notter, R. H., J. N. Finkelstein, and R. D. Taubold. 1983. Comparative adsorption of natural lung surfactant, extracted phospholipids, and artificial phospholipid mixtures to the air-water interface. *Chem. Phys. Lipids.* 33:67–80.
27. Hall, S. B., Z. Wang, and R. H. Notter. 1994. Separation of subfractions of the hydrophobic components of calf lung surfactant. *J. Lipid Res.* 35:1386–1394.
28. Takahashi, A., and T. Fujiwara. 1986. Proteolipid in bovine lung surfactant: its role in surfactant function. *Biochem. Biophys. Res. Commun.* 135:527–532.
29. Hawgood, S., B. J. Benson, …, R. T. White. 1987. Nucleotide and amino acid sequences of pulmonary surfactant protein SP 18 and evidence for cooperation between SP 18 and SP 28-36 in surfactant lipid adsorption. *Proc. Natl. Acad. Sci. USA.* 84:66–70.
30. Kaplan, R. S., and P. L. Pedersen. 1985. Determination of microgram quantities of protein in the presence of milligram levels of lipid with amido black 10B. *Anal. Biochem.* 150:97–104.
31. Ames, B. N. 1966. Assay of inorganic phosphate, total phosphate and phosphatases. *Methods Enzymol.* 8:115–118.
32. Kumar, K., M. Chavarha, …, S. B. Hall. 2018. The Lγ phase of pulmonary surfactant. *Langmuir.* 34:6601–6611.
33. Liu, S., L. Zhao, …, G. A. Lajoie. 2008. Characterization of bovine surfactant proteins B and C by electrospray ionization mass spectrometry. *Rapid Commun. Mass Spectrom.* 22:197–203.
34. Schram, V., and S. B. Hall. 2001. Thermodynamic effects of the hydrophobic surfactant proteins on the early adsorption of pulmonary surfactant. *Biophys. J.* 81:1536–1546.
35. Markin, C. J., and S. B. Hall. 2020. The anionic phospholipids of bovine pulmonary surfactant. *Lipids*, Published online Sept. 7, 2020.
36. Tristram-Nagle, S. A. 2007. Preparation of oriented, fully hydrated lipid samples for structure determination using X-ray scattering. *Methods Mol. Biol.* 400:63–75.
37. Mills, T. T., S. Tristram-Nagle, …, G. W. Feigenson. 2008. Liquid-liquid domains in bilayers detected by wide angle X-ray scattering. *Biophys. J.* 95:682–690.
38. Mills, T. T., G. E. Toombes, …, J. F. Nagle. 2008. Order parameters and areas in fluid-phase oriented lipid membranes using wide angle X-ray scattering. *Biophys. J.* 95:669–681.
39. Lemmich, J., K. Mortensen, …, O. G. Mouritsen. 1995. Pseudocritical behavior and unbinding of phospholipid bilayers. *Phys. Rev. Lett.* 75:3958–3961.
40. Szekely, P., T. Dvir, …, U. Raviv. 2011. Effect of temperature on the structure of charged membranes. *J. Phys. Chem. B.* 115:14501–14506.
41. Loney, R. W., S. Panzuela, …, S. A. Tristram-Nagle. 2020. Location of the hydrophobic surfactant proteins, SP-B and SP-C, in fluid-phase bilayers. *J. Phys. Chem. B.* 124:6763–6774.
42. Liu, Y., and J. F. Nagle. 2004. Diffuse scattering provides material parameters and electron density profiles of biomembranes. *Phys. Rev. E. Stat. Nonlin. Soft Matter Phys.* 69:040901.
43. Tristram-Nagle, S., R. Zhang, …, J. F. Nagle. 1993. Measurement of chain tilt angle in fully hydrated bilayers of gel phase lecithins. *Biophys. J.* 64:1097–1109.
44. Patterson, A. L. 1939. The Scherrer formula for X-ray particle size determination. *Phys. Rev.* 56:978–982.
45. Tristram-Nagle, S., M. C. Wiener, …, J. F. Nagle. 1987. Kinetics of the subtransition in dipalmitoylphosphatidylcholine. *Biochemistry.* 26:4288–4294.
46. Biltonen, R. L., and D. Lichtenberg. 1993. The use of differential scanning calorimetry as a tool to characterize liposome preparations. *Chem. Phys. Lipids.* 64:129–142.
47. Mills, T. T., J. Huang, …, J. F. Nagle. 2009. Effects of cholesterol and unsaturated DOPC lipid on chain packing of saturated gel-phase DPPC bilayers. *Gen. Physiol. Biophys.* 28:126–139.

48. Discher, B. M., K. M. Maloney, …, S. B. Hall. 1999. Neutral lipids induce critical behavior in interfacial monolayers of pulmonary surfactant. *Biochemistry.* 38:374–383.

49. Discher, B. M., K. M. Maloney, …, S. B. Hall. 2002. Effect of neutral lipids on coexisting phases in monolayers of pulmonary surfactant. *Biophys. Chem.* 101–102:333–345.

50. Veatch, S. L., O. Soubias, …, K. Gawrisch. 2007. Critical fluctuations in domain-forming lipid mixtures. *Proc. Natl. Acad. Sci. USA.* 104:17650–17655.

51. Katsaras, J., V. A. Raghunathan, …, J. Dufourcq. 1995. Evidence for a two-dimensional molecular lattice in subgel phase DPPC bilayers. *Biochemistry.* 34:4684–4688.

52. Stefaniu, C., I. Vilotijevic, …, P. H. Seeberger. 2012. Subgel phase structure in monolayers of glycosylphosphatidylinositol glycolipids. *Angew. Chem. Int. Ed. Engl.* 51:12874–12878.

53. Piknova, B., V. Schram, and S. B. Hall. 2002. Pulmonary surfactant: phase behavior and function. *Curr. Opin. Struct. Biol.* 12:487–494.

54. Jähnig, F. 1984. Lipid exchange between membranes. *Biophys. J.* 46:687–694.

55. Nagle, J. F. 1986. Theory of lipid monolayer and bilayer chain-melting phase transitions. *Faraday Discuss. Chem. Soc.* 81:151–162.

56. Feng, S. S. 1999. Interpretation of mechanochemical properties of lipid bilayer vesicles from the equation of state or pressure - area measurement of the monolayer at the air - water or oil - water interface. *Langmuir.* 15:998–1010.

57. Marsh, D. 1996. Lateral pressure in membranes. *Biochim. Biophys. Acta.* 1286:183–223.

58. Schief, W. R., M. Antia, …, V. Vogel. 2003. Liquid-crystalline collapse of pulmonary surfactant monolayers. *Biophys. J.* 84:3792–3806.

59. Lee, K. Y. C. 2008. Collapse mechanisms of Langmuir monolayers. *Annu. Rev. Phys. Chem.* 59:771–791.

60. Yan, W., and S. B. Hall. 2006. Distribution of coexisting solid and fluid phases alters the kinetics of collapse from phospholipid monolayers. *J. Phys. Chem. B.* 110:22064–22070.

61. Zuo, Y. Y., S. M. Tadayyon, …, F. Possmayer. 2008. Atomic force microscopy studies of functional and dysfunctional pulmonary surfactant films, II: albumin-inhibited pulmonary surfactant films and the effect of SP-A. *Biophys. J.* 95:2779–2791.

62. Bernardino de la Serna, J., J. Perez-Gil, …, L. A. Bagatolli. 2004. Cholesterol rules: direct observation of the coexistence of two fluid phases in native pulmonary surfactant membranes at physiological temperatures. *J. Biol. Chem.* 279:40715–40722.

63. Sachan, A. K., and J. A. Zasadzinski. 2018. Interfacial curvature effects on the monolayer morphology and dynamics of a clinical lung surfactant. *Proc. Natl. Acad. Sci. USA.* 115:E134–E143.

64. Putz, G., J. Goerke, and J. A. Clements. 1994. Surface activity of rabbit pulmonary surfactant subfractions at different concentrations in a captive bubble. *J. Appl. Physiol.* 77:597–605.

65. Schürch, D., O. L. Ospina, …, J. Pérez-Gil. 2010. Combined and independent action of proteins SP-B and SP-C in the surface behavior and mechanical stability of pulmonary surfactant films. *Biophys. J.* 99:3290–3299.

66. Dagan, M. P., and S. B. Hall. 2015. The equilibrium spreading tension of pulmonary surfactant. *Langmuir.* 31:13063–13067.

67. Xu, L., Y. Yang, and Y. Y. Zuo. 2020. Atomic force microscopy imaging of adsorbed pulmonary surfactant films. *Biophys. J.* 119:756–766.

68. Ueda, S., N. Ishii, …, M. Okayasu. 1983. Ultrastructural studies on surface lining layer of the lungs. Part II. *J. Jpn. Med. Soc. Biol. Interface.* 14:24–46.

69. Hills, B. A. 1988. The Biology of Surfactant. Cambridge University Press, New York, pp. 222–235.

70. Al-Saiedy, M., A. Tarokh, …, M. Amrein. 2017. The role of multilayers in preventing the premature buckling of the pulmonary surfactant. *Biochim. Biophys. Acta Biomembr.* 1859:1372–1380.

71. Follows, D., F. Tiberg, …, M. Larsson. 2007. Multilayers at the surface of solutions of exogenous lung surfactant: direct observation by neutron reflection. *Biochim. Biophys. Acta.* 1768:228–235.